JOURNAL OF AIRCRAFT
Vol. 41, No. 6, November–December 2004

Numerical Analyses of Discrete Gust Response for an Aircraft

Guowei Yang*
Chinese Academy of Sciences, 100080 Beijing, People's Republic of China
and
Shigeru Obayashi†
Tohoku University, 980-8577 Sendai, Japan

Based on Navier–Stokes equations and structural and flight dynamic equations of motion, dynamic responses in vertical discrete gust flow perturbation are investigated for a supersonic transport model. A tightly coupled method was developed by subiterations between aerodynamic equations and dynamic equations of motion. First, under the assumption of rigid-body and single freedom of motion in the vertical plunging, the results of a direct-coupling method are compared with the results of quasi-steady model method. Then, gust responses for the one-minus-cosine gust profile are analyzed with two freedoms of motion in plunging and pitching for the airplane configurations with and without the consideration of structural deformation.

Introduction

GUST load is one of the important dynamic loads considered in aircraft structure design. Because of its multidisciplinary nature with aerodynamics, flight dynamics, aeroelasticity, and atmospheric turbulence, until now, only the doublet-lattice, unsteady linear aerodynamic code DLM, coupled with the equation of motion of flexible vehicle, was used for gust response analysis.[1–3]

Gusts in nature tend to be random. The early design methods for gust loads were based on a single discrete gust having a one-minus-cosine velocity profile. Recently, the statistical discrete gust method and the power spectral density method[4] in the frequency domain have been used to define the gust loads, however, which are still hard to combine with the modern Navier–Stokes numerical method.

In recent years, for the motion of rigid vehicles, the path of stores during the separation phase has mainly been investigated with the computational fluid dynamics (CFD) algorithm coupled with a six-degree-of-freedom (6DOF) algorithm.[5–8] For the motion of a flexible body, only Leishman and his team at the University of Maryland did this kind of work for the rotor blades. Insofar as the authors know, the computation of gust response with the coupling method has still not been reported. In this paper, the fully implicit multiblock Navier–Stokes aeroelastic solver implemented by Yang et al.,[9] coupled with the flight and structural dynamic equations of motion, has been developed to simulate gust dynamic responses, which can model the motion of rigid or flexible vehicles. Because it is hard to find the structural data of a flexible vehicle, the supersonic transport (SST) designed by National Aerospace Laboratory of Japan (NAL),[10] which has high rigidity, is taken as our calculated case. To study the effects of dynamic response due to flow perturbation and airplane motion, which involves only the consideration of vertical plunging motion, a comparative study was first done for the airplane in the harmonic flow perturbation with the direct-coupling method and the quasi-steady model method. Then, the gust responses in a one-minus-cosine gust velocity profile are analyzed with two freedoms of motion in plunging and pitching, with and without the consideration of structural deformation.

Received 18 May 2003; presented as Paper 2003-3513 at the 21st Applied Aerodynamics Conference, Orlando, FL, 23 June 2003; revision received 7 February 2004; accepted for publication 9 February 2004.

*Professor, Key Laboratory of High-Temperature Gas Dynamics, Institute of Mechanics.
†Professor, Institute of Fluid Science. Associate Fellow AIAA.

Aerodynamic Equations and Numerical Method

Aerodynamic governing equations are the unsteady, three-dimensional, thin-layer Navier–Stokes equations in strong conservation law form, which can be written in curvilinear coordinates as

$$\partial_t \hat{Q} + \partial_\xi F + \partial_\eta G + \partial_\zeta H = \partial_\zeta H_v + S_{\mathrm{GCL}} \tag{1}$$

The source term S_{GCL} is obtained from the geometric conservation law (GCL) for a moving mesh.[11] In the formulation, all variables are normalized by the appropriate combination of freestream density, freestream velocity, and mean aerodynamic chord length. The viscosity coefficient μ in H_v is computed as the sum of laminar and turbulent viscosity coefficients, which are evaluated by Sutherland's law and the Baldwin–Lomax model.[12]

The lower-upper symmetric Gauss–Seidel (LU-SGS) method (see Ref. 13), employing a Newton-like subiteration, is used for the solution of Eq. (1). Second-order temporal accuracy is obtained by utilization of a three-point backward difference in the subiteration procedure. The numerical algorithm can be deduced as

$$LD^{-1}U\,\Delta Q = -\phi^i\left\{(1+\phi)Q^p - (1+2\phi)Q^n + \phi Q^{n-1} - J\,\Delta t\,Q^p S^p_{\mathrm{GCL}} + J\,\Delta t\left[\delta_\xi F^p + \delta_\eta G^p + \delta_\zeta\left(H^p - H^p_v\right)\right]\right\} \tag{2}$$

where

$$L = \bar{\rho} I + \phi^i J\,\Delta t\left(A^+_{i-1,j,k} + B^+_{i,j-1,k} + C^+_{i,j,k-1}\right), \qquad D = \bar{\rho} I$$

$$U = \bar{\rho} I - \phi^i J\,\Delta t\left(A^-_{i+1,j,k} + B^-_{i,j+1,k} + C^-_{i,j,k+1}\right)$$

$$\bar{\rho} = 1 + \phi^i J\,\Delta t\left[\bar{\rho}(A) + \bar{\rho}(B) + \bar{\rho}(C)\right], \qquad \phi^i = 1/(1+\phi)$$

$$\Delta Q = Q^{p+1} - Q^p$$

Here, $\phi = 0.5$, and Q^p is the subiteration approximation to Q^{n+1}. As $p \to \infty$, $Q^p \to Q^{n+1}$. The deduced subiteration scheme reverts to the standard first-order LU-SGS scheme for $\phi = 0$ and $p = 1$.

The inviscid terms in Eq. (1) are approximated by the modified third-order upwind HLLEW scheme of Obayashi and Guruswamy.[14] For the isentropic flow, the scheme results in the standard upwind-biased flux-difference splitting scheme of Roe, and as the jump in entropy becomes large in the flow, the scheme turns into the standard HLLEW scheme. The thin-layer viscous term in Eq. (1) is discretized by second-order central difference.

For multiblock-grid applications, the Navier–Stokes equations are solved in each block separately. To calculate the convective and viscous fluxes in the block boundary, data communication is

performed through two-level halo cells. The details about the multiblock Navier–Stokes solver can be found in Refs. 5 and 15.

Equations of Motion and Numerical Method

In the present study of dynamic response, the airplane is given freedom in vertical plunging and pitching, and the following assumptions are made:

1) The disturbed motion is symmetrical with respect to the airplane's longitudinal plane of symmetry.

2) The airplane is initially in horizontal flight at cruise velocity.

3) The vertical gust perturbation is normal to the flight path and is uniform in the spanwise direction.

4) For the consideration of structural deformation, only the structural deformation of the wing is considered, and its deformation is approximated to the elastic plate model.

Direct-Coupling Method

With the preceding assumptions, the equilibriums of total force along the z axis and total pitching moment about the y axis are

$$\iint_S \ddot{w}(x, y, t)\rho \, dx \, dy = \iint_S \Delta p(x, y, t) \, dx \, dy \tag{3a}$$

$$\iint_S \ddot{w}(x, y, t)\rho x \, dx \, dy = \iint_S \Delta p(x, y, t) x \, dx \, dy \tag{3b}$$

For the equilibrium of an element, we obtain

$$w(x, y, t) - w(0, 0, t) - x\frac{\partial w(0, 0, t)}{\partial x} = \iint_S C(x, y; \xi, \eta) \times [\Delta p(\xi, \eta, t) - \rho(\xi, \eta)\ddot{w}(\xi, \eta, t)] \, d\xi \, d\eta \tag{3c}$$

In the system of equations, the unknown quantity $w(x, y, t)$ represents the disturbed displacement of elastic airplane from its original equilibrium state. The pressure change of $\Delta p(x, y, t)$ based on cruise condition is calculated by the unsteady aerodynamic equations, which depends on the instantaneous values of displacement, velocity, acceleration of the airplane, as well as the past history of the motion.

Introducing natural modes with the Rayleigh–Ritz method (see Ref. 16) we have

$$w(x, y, t) = \sum_{i=1}^{n} \phi_i(x, y) q_i(t) \tag{4}$$

where $\phi_i(x, y)$ are normalized natural mode shapes of the airplane, including rigid modes, and $q_i(t)$ is generalized displacement. Then Eqs. (3a–3c) can be reduced to

$$\ddot{q}_i + 2\zeta_i\omega_i\dot{q}_i + \omega_i^2 q_i = F_i/M_i, \qquad i = 1, 2, \ldots, n, \qquad \omega_1 = \omega_2 = 0 \tag{5}$$

with the initial conditions $q_i(0) = \dot{q}_i(0) = 0$, where

$$M_i = \iint_S \phi_i^2(x, y)\rho(x, y) \, dx \, dy$$

$$F_i = \iint_S \Delta p(x, y, t)\phi_i(x, y) \, dx \, dy$$

The first equation in Eq. (5) is the equation of motion in vertical plunging. In Eq. (5), the generalized mass M_1 represents the mass of airplane and q_1 the plunging displacement. Similarly, the second equation is the equation of motion in pitching. M_2 and q_2 represent the pitching moment of inertia and angular displacement in pitching, respectively, and ω_i and ς_i are the natural frequency of structural modes and the damping ratio in the ith mode, which are zero for the first two equations of motion of rigid body.

The subiteration method can also be used for Eq. (5). The resulting numerical scheme is

$$\begin{bmatrix} 1 & -\phi^i \Delta t \\ \phi^i \Delta t \omega_i^2 & 1 + 2\phi^i \omega_i \zeta_i \Delta t \end{bmatrix} \Delta S = -\phi^i \left\{ (1+\phi)S^p - (1+2\phi)S^n + \phi S^{n-1} + \Delta t \begin{bmatrix} 0 & -1 \\ \omega_i^2 & 2\omega_i\zeta_i \end{bmatrix} S^p - \Delta t \begin{bmatrix} 0 \\ F_i^p/M_i \end{bmatrix} \right\} \tag{6}$$

where $S = [q, \dot{q}]$ and $\Delta S = S^{p+1} - S^p$.

As $p \to \infty$, a fully implicit second-order temporal accuracy scheme for the numerical simulation of dynamic response is formed by coupling solutions of Eqs. (2) and (6). Numerical experiments[17] indicate, in general, that the calculated results are nearly unchangeable when $p \geq 3$. In the following calculation, the number of subiteration is set to three.

If the airplane is assumed as the rigid body, then only the first two equations of Eq. (5), coupled with the aerodynamic equations, need to be solved. If the pitching motion can be further neglected, the dynamic response is only considered in the motion of vertical plunging. For the simpler case, the quasi-steady model method can be introduced as follows.

Quasi-Steady Model Method

If the time lag in buildup of lift is neglected and the incremental lift is considered only due to the change of angle of attack, then the model equation of motion can be written simply as

$$M\ddot{z} = \tfrac{1}{2}\rho_\infty V_\infty^2 S C_{L\alpha}\{[w(t)/V_\infty] - \dot{z}/V_\infty\} \tag{7}$$

Here, $w(t)$ represents the vertical perturbation velocity profile. The normalized equation can be written as

$$\ddot{z} + C_1 C_{L\alpha}\dot{z} = C_1 C_{L\alpha} w(t) \tag{8}$$

where $C_1 = \rho_\infty Sc/2M$. $C_{L\alpha}$ is the derivative of lift coefficient that can be determined by either steady flow calculation or wind-tunnel experiment. Through the comparison of this method with the direct-coupling method, the dynamic responses under the quasi-steady assumption can be studied.

Results and Discussions

Dynamic responses in vertical flow perturbation are studied for the SST experimental model[9] shown in Fig. 1. For the experimental aircraft, the fuselage length is 11.5 m, the mean aerodynamic chord 2.754 m, the reference area $S = 10.12$ m^2, the weight 1950 kg, the center of gravity from the head of the airplane 6.05266 m, and the pitching moment of inertia $I_{yy} = 10632$ kgm^2. The design cruise point is at $M_\infty = 2.0$, $\alpha = 2$ deg, and $Re = 27.5 \times 10^6$, and the flight altitude 15,000 m. For the solution of structural deformation, the data of the structural oscillating natural modes and frequencies are provided by the NAL. The first five structural modes and natural frequencies are shown in Fig. 2. The aircraft is initially assumed

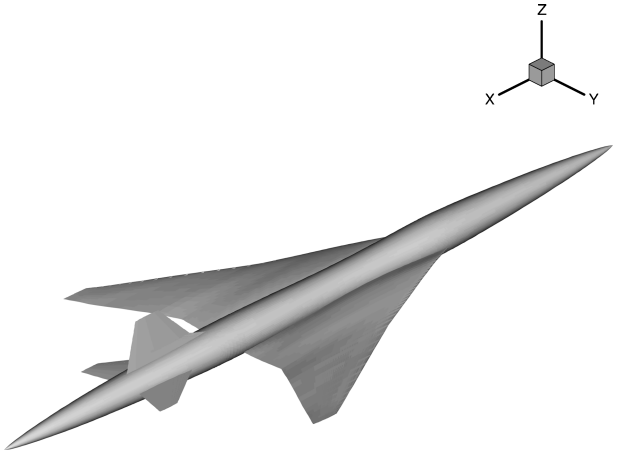

Fig. 1 SST configuration.

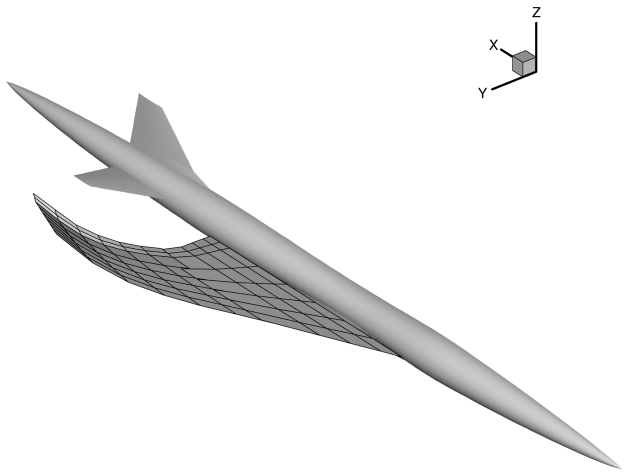

a) Mode 1, $f_1 = 485.5$ Hz

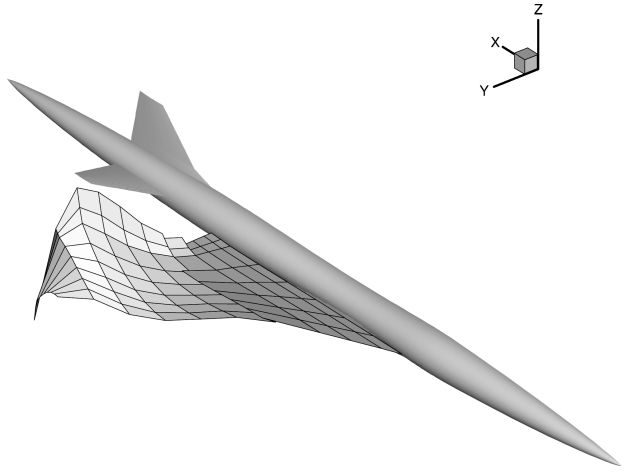

c) Mode 3, $f_3 = 2121.1$ Hz

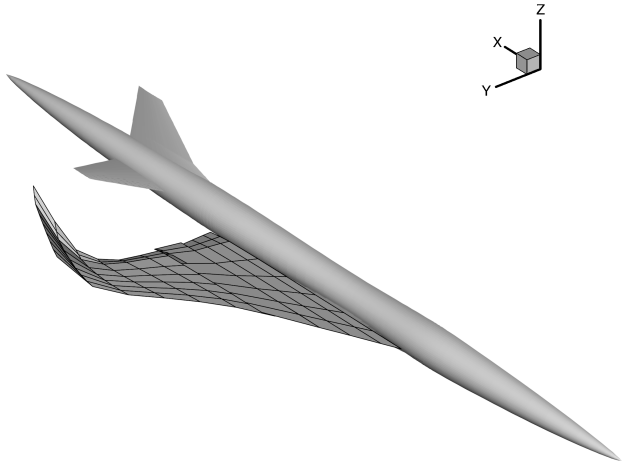

b) Mode 2, $f_2 = 1207.1$ Hz

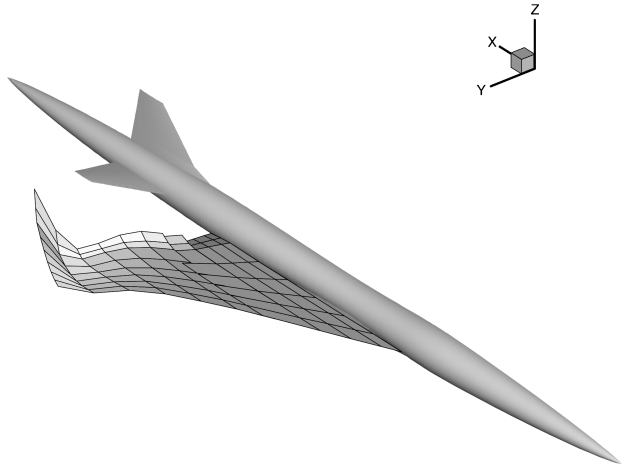

d) Mode 4, $f_4 = 2489.1$ Hz

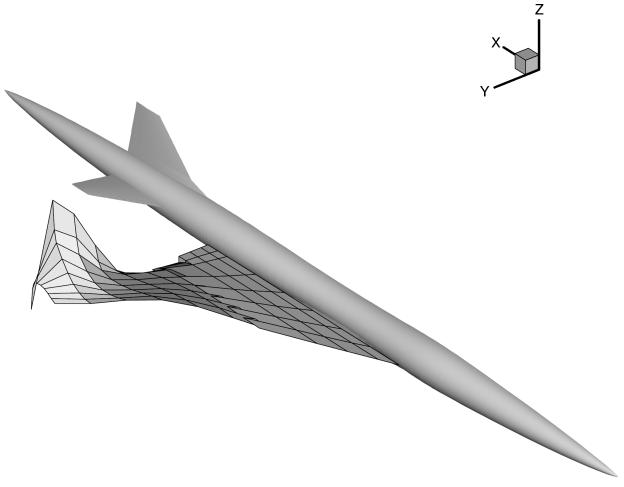

e) Mode 5, $f_5 = 3272.3$ Hz

Fig. 2 First five modes and natural frequencies for SST structural model.

at cruise flight and then encounters a gust turbulence atmosphere. Hence, the calculation of gust dynamic response needs to start from the cruise steady flowfield.

The H–H type multiblock grid with 30 blocks was generated for the SST configuration shown in Fig. 3. The comparison of the predicted coefficients of lift, drag, and pitching moment with the experimental data of wind tunnel is shown in Fig. 4. The agreement between experiment and calculation is fairly good; however, it is still hard for us to explain why the predicted slopes of lift and moment curves are larger slightly than the experiment and why the drag does not match well at some angles of attacks, as well. The cruise lift coefficient at a cruise condition of $M_\infty = 2.0$ and $\alpha = 2$ deg is calculated as $C_{L0} = 0.112$, which corresponds with the experimental value of 0.110. For the quasi-steady model equation of motion (7), the derivative of lift coefficient needs to be known. Based on the curve of lift coefficient, the derivative can be approximately calculated as $C_{L\alpha} = 2.15$.

In Ref. 9, the pitching LANN wing and the standard aeroelastic AGARD 445.6 wing have been used to validate the unsteady CFD code and the algorithm of deforming grid. The following results can be thought of as reasonable even though no unsteady experimental data are presented for comparison.

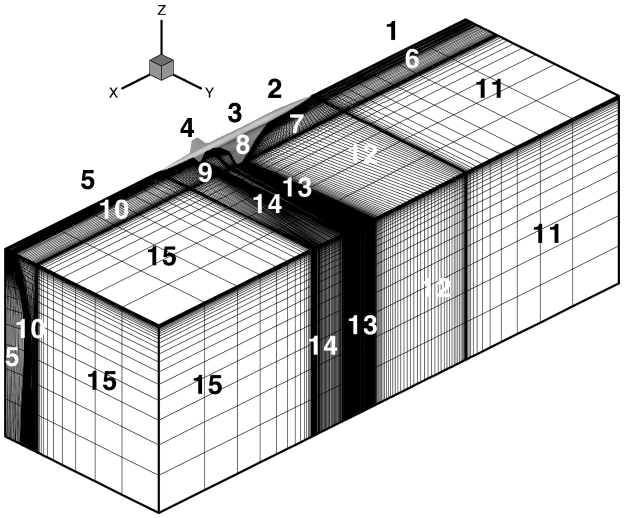

Fig. 3 Multiblock grid with 30 blocks for SST.

Dynamic Response for Harmonic Perturbation

The SST experimental model is designed for cruise at $M_\infty = 2.0$ and $\alpha = 2$ deg and a flight altitude of 15,000 m. A future SST is expected to cruise at a supersonic speed only over the sea and to cruise at a transonic speed over land. Because of the strong nonlinearity of transonic flows, the transonic dynamic response may be of interest. We assume that the experimental airplane can cruise at $M_\infty = 0.9$ and a flight altitude of 9000 m. At cruise flight, because of the equilibrium of various forces and moments, the cruise lift should be equal to the total weight of airplane. Therefore, the cruise angle of attack $\alpha = 2.14$ deg at $M_\infty = 0.9$ can be calculated based on the curve of lift vs angles of attack. The numerical results also show that the pitching moment about the gravity center of the airplane still exists for this case. In fact, to guarantee the cruise of the airplane at transonic Mach number, the high-lift system and the empennage deflection should be used to keep the equilibrium of forces and moments; however, these influences are not considered in the paper.

A vertical harmonic flow perturbation is added to the steady flow of the aircraft at $M_\infty = 0.9$ and $\alpha = 2.14$ deg with

$$w(t) = w_0 \sin(\omega t) \tag{9}$$

The amplitude of the flow perturbation is set at $w_0 = 50$ ft/s = 15.24 m/s and the reduced frequency $k = \omega c / V_\infty = \pi / 12.5$, which correspond with the design cruise gust speed (effect of altitude is not considered) and the frequency of one-minus-cosine discrete gust profile.[4]

The quasi-steady model method is decided by a second-order ordinary equation of Eq. (7). Its initial conditions can be assumed as $z_{t=0} = 0$ and $\dot{z}_{t=0} = 0$. After the slope of lift curve and gust profile are given, then the time histories of vertical displacement $z(t)$, the change of angle of attack due to motion $\Delta\alpha(t) \approx \dot{z}(t)/V_\infty$, and the incremental load factor $\Delta n(t) = \ddot{z}(t)/g$ are calculated. The direct-coupling method is used to derive a time-accurate solution by the use of a coupled unsteady CFD code with the equation of plunging motion and direct use of a gust profile. Figure 5 shows the time histories of two methods. The dynamic responses of the quasi-steady model method after the translation of lag time are also depicted in Fig. 5. Overall frequency responses of the two methods, whose nondimensional value is about 0.04, are nearly the same. The incremental load factor (equivalent to the lift coefficient) has no large change except at the position of the minimum, but by comparison of the direct-coupling method, the quasi-steady method predicts the slower growth of displacement with time and the opposite tendency of change of angle of attack. On the other hand, the vertical displacement grows near linearly with time, which is contrary to its actual tendency. Therefore, the effect of pitching motion should be considered. We know that only the direct-coupling method can treat multifreedom motions.

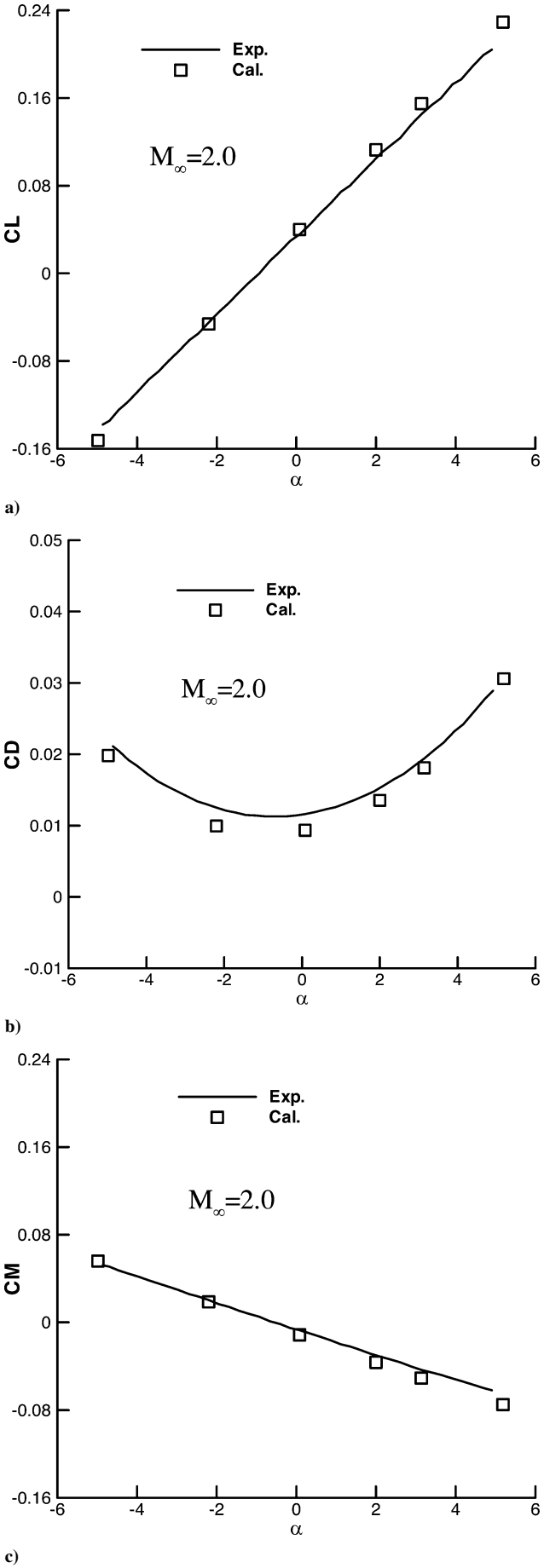

Fig. 4 Comparison of the predicted lift, drag, and pitching moment coefficients with wind-tunnel experiments.

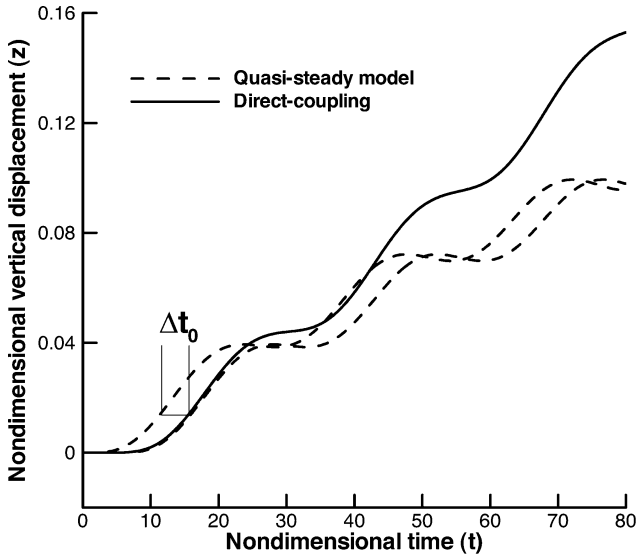

a)

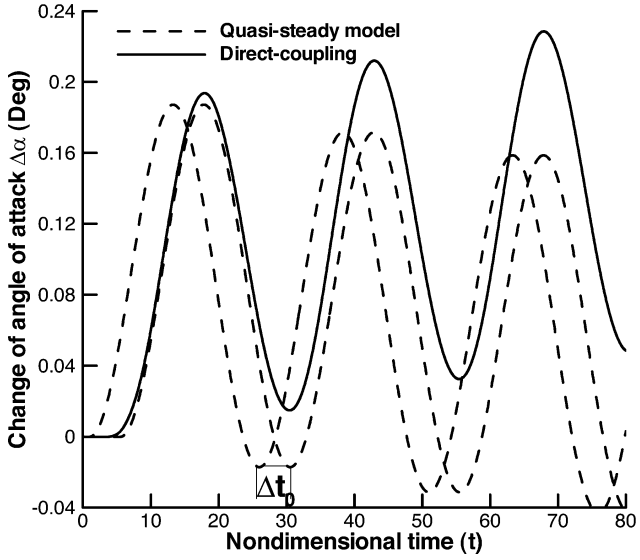

b)

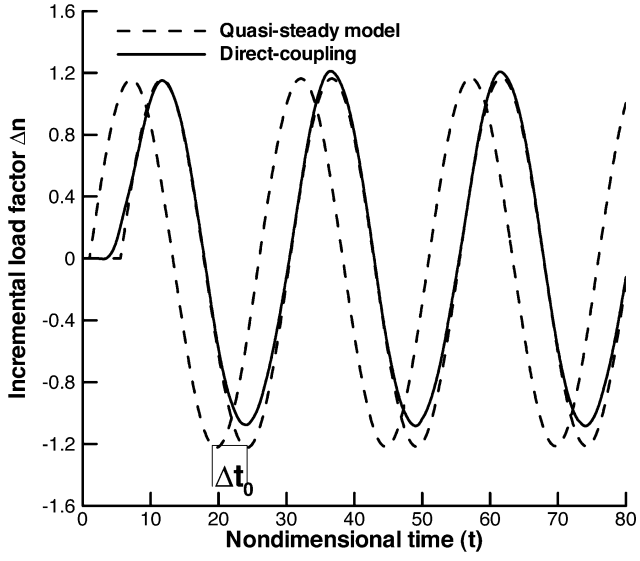

c)

Fig. 5 Time histories of vertical displacement, angle of attack, and incremental load factor for SST at $M_\infty = 0.9$ and $\alpha = 2.14$ deg.

Supersonic dynamic response at $M_\infty = 2.0$ has also been calculated (not shown in here), which behaves differently. The results show nearly no difference for the quasi-steady model and the direct-coupling method. This indicates that in supersonic dynamic response, the contribution for buildup of lift due to airplane motion is small and can be neglected.

Dynamic Response for One-Minus-Cosine Gust

The early design methods for gust loads were based on the discrete gust having one-minus-cosine velocity profile, namely,

$$W_g = \tfrac{1}{2} W_0[1 - \cos(2\pi x/2H)] \tag{10}$$

W_0 is the design cruise gust velocity, specified as 50 ft/s at the altitudes from sea level to 20,000 ft. It then decreases linearly as the functions of altitudes.[4] In the present calculation of cruise altitude of 9000 m, W_0 is assumed as 50 ft/s. The gust gradient distance H is taken as the 12.5 times mean geometric chord lengths based on the experimental evidence.[4] Before and after the discrete gust pulse, there is no gust flow perturbation. This velocity profile is shown in Fig. 6. In the following discussion, we need to study how the airplane moves in plunging and pitching, how the loads change, and how the structure deforms under the discrete gust profile. In the paper, a total of four cases, rigid plus plunge, flexible plus plunge rigid plus plunge plus pitch, and flexible plus plunge plus pitch are simulated. The fourth case is the most complicated case, which is needed to simulate simultaneously the motion of the aircraft in plunging and pitching as well as its structural deformation.

The time histories of the load coefficients of lift, drag, pitching moment, and bending moment are shown in Fig. 7, which indicates that the loads are nearly unchangeable with or without the consideration of structural deformation due to the stronger structural rigidity of the SST. When the airplane flies through the gust pulse, forces and moments also experience a pulse, but a slightly larger maximum load is predicted without consideration of the motion in pitching. After the pulse response, the loads tend to recover to the equilibrium state or to emerge to oscillate in decay for the methods with and without the consideration of the motion in pitching. The overall nondimensional response frequency is about 0.012.

The displacement in plunging and the angular displacement in pitch are shown in Fig. 8. Without the consideration of motion in pitching, the displacement in plunging increases nearly linearly with time, which is obviously contrary to its actual tendency. Similar to the preceding analyses of harmonic perturbation, the method without the pitching motion cannot simulate the response motion of the aircraft correctly. When the airplane motion in plunging and pitching are considered, the responses of the airplane appear to be two

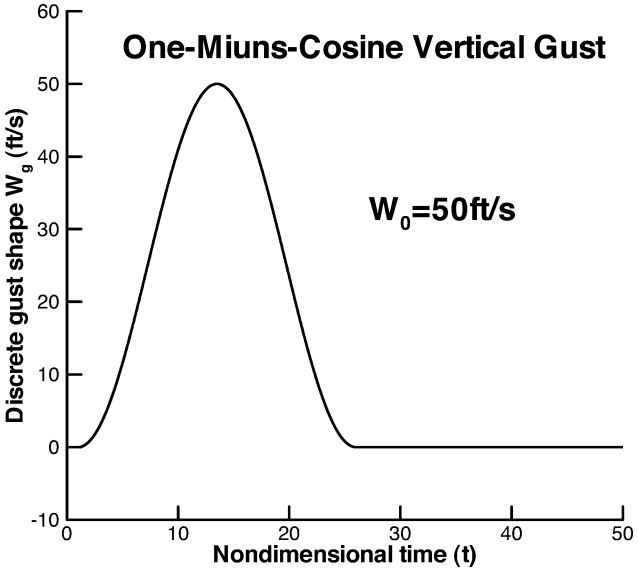

Fig. 6 One-minus-cosine gust velocity profile.

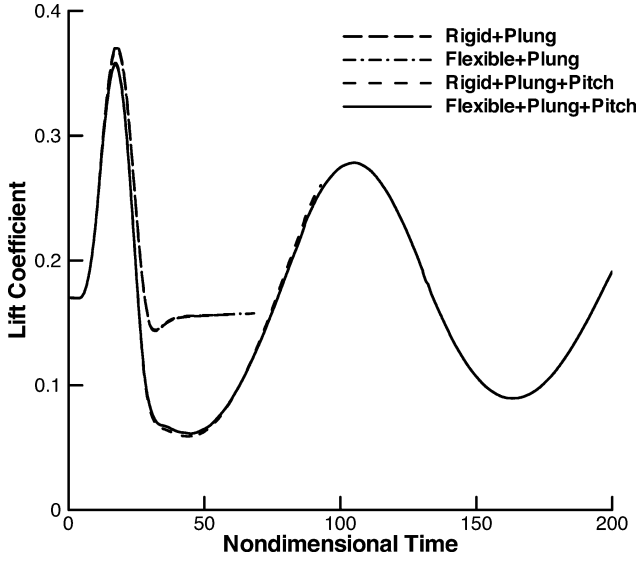

a)

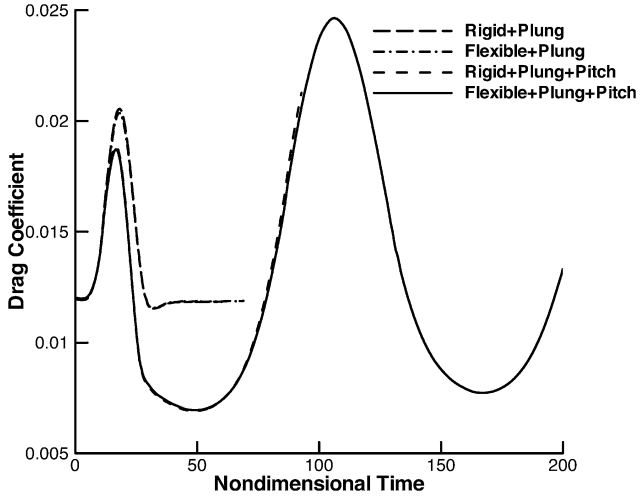

b)

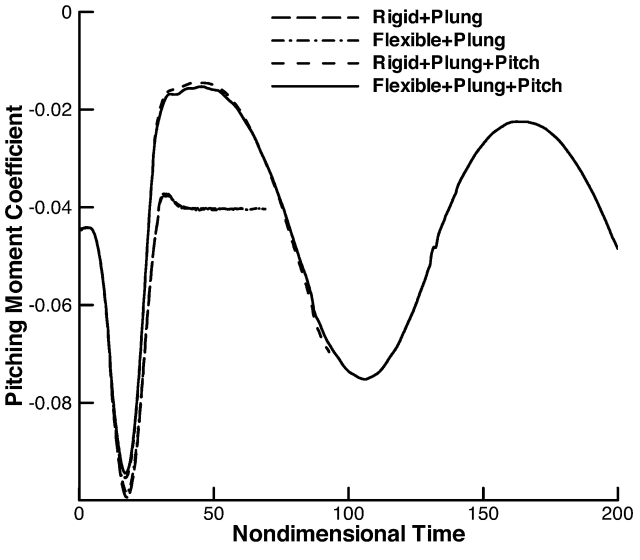

c)

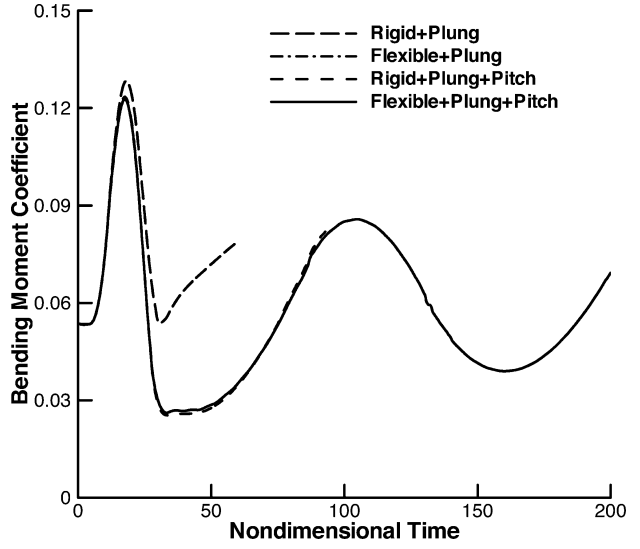

d)

Fig. 7 Time histories of the coefficients of lift, drag, pitching moment, and bending moment for rigid and flexible configurations at $M_\infty = 0.9$ and $\alpha = 2.14$ deg.

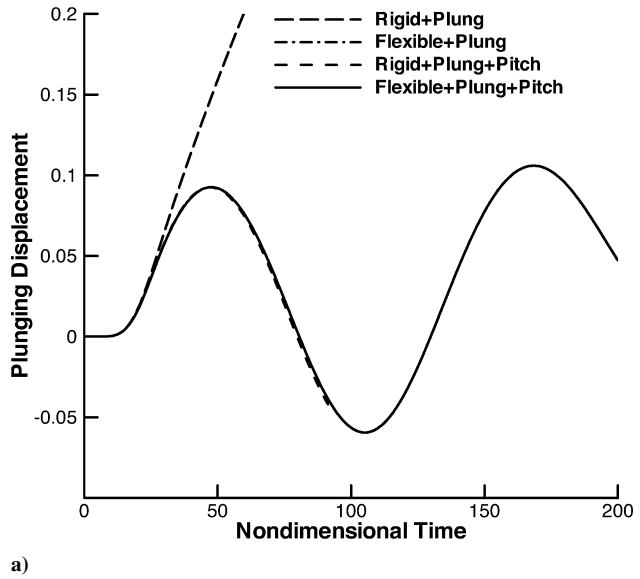

a)

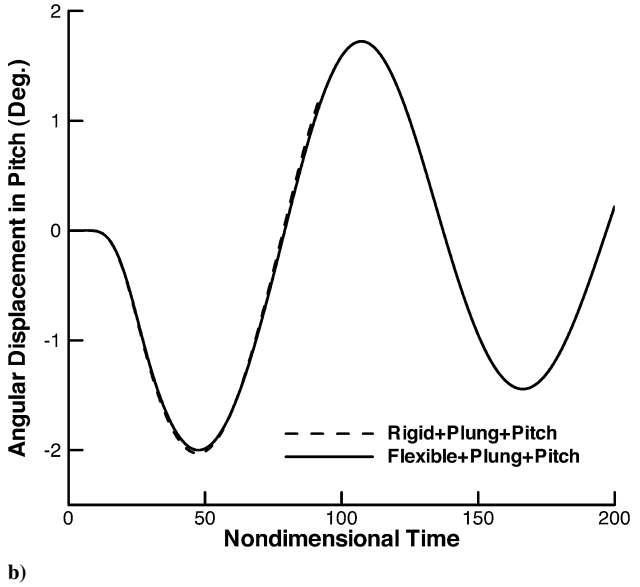

b)

Fig. 8 Time histories of the vertical plunging displacement and angular displacement in pitch for rigid and flexible configurations at $M_\infty = 0.9$ and $\alpha = 2.14$ deg.

freedoms of oscillation. As the airplane plunges up, the airplane pitches down simultaneously. This can be used for the explanation of the change of loads in Fig. 7 in the corresponding phase, namely, due to the decrease of angle of attack, the lift, drag, and bending moments decrease and pitching moment increases. On the contrary, when the airplane plunges down and pitches up, due to the increase of angle of attack, the lift, drag, and bending moment increase and the pitching moment decreases. The maximum amplitudes of the plunging and pitching oscillation are about 0.1 times mean aerodynamic chord length and 1.8 deg, respectively. The numerical results also show that the pitching oscillation decays much faster than the plunging oscillation does.

Figure 9 gives the time histories of structural deformation of the generalized displacements. The structural deformation occurs mainly in the first two modes, which corresponds to the first and second bending modes of Figs. 2a and 2b. Although the deformation is smaller, the airplane experiences a larger structural deformation in the gust process, which has the same changeable tendency of the lift coefficient in Fig. 7a. After the pulse response, structural deformation oscillates to revert to the original equilibrium state without consideration of the motion in pitching and with two freedoms of motion. The structural deformation oscillates in a much more complicated manner, which couples the natural structural oscillation of high frequency and the airplane motion of a long period in plunging and pitching. The nondimensional value of high frequency is 0.158, and the low frequency of the aircraft motion is 0.012, which is the same as the frequency of load responses. Finally, through comparison of responses with and without pitching motion, we know that both methods simulated a completely different response process of structural deformation after the gust pulse.

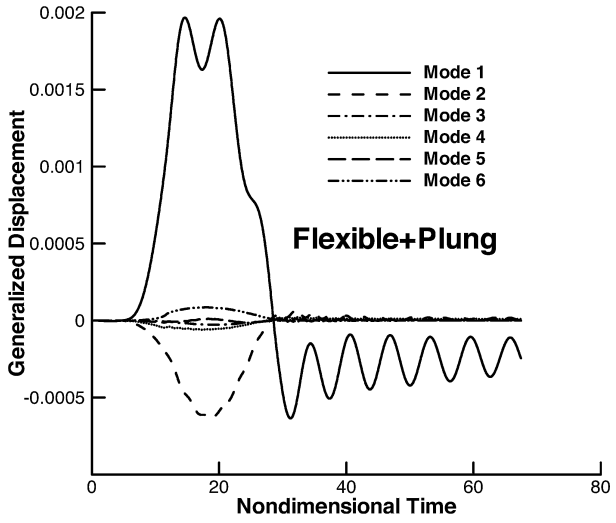

a)

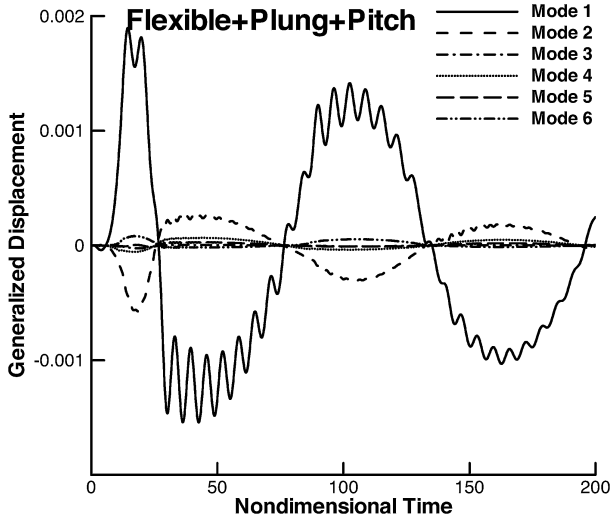

b)

Fig. 9 Time histories of structural deformation of the first six modes for the flexible configuration with and without the pitching motion at $M_\infty = 0.9$ and $\alpha = 2.14$ deg.

Conclusions

In the present paper, a solver for the analysis of discrete gust response was developed through the coupling solution of Navier–Stokes equations and structural and flight dynamic equations of motion. The gust responses for the SST model have been analyzed with the developed solver. Numerical results indicate that if the loads and structural deformation experience a larger pulse change in the discrete gust process, the airplane appears to have two freedoms of oscillation in plunging and pitching. The responses of structural modes contain two frequencies, namely, the high frequency of natural structural oscillation and the low frequency of aircraft motion. Because of the stronger rigidity for the SST structural model, there is nearly no influence on the loads and motions of the aircraft with or without the consideration of structural deformation.

Acknowledgments

Structural data of the supersonic transport model were provided by Jiro Nakamichi of National Aerospace Laboratory of Japan. This work is supported by the National Science Foundation of China, 10372106.

References

[1]Perry, B., III, Pototzky, A. S., and Woods, J. A., "NASA Investigation of a Claimed 'Overlap' Between Two Gust Response Analysis Methods," *Journal of Aircraft*, Vol. 27, No. 7, 1990, pp. 605–611.

[2]Scott, R. C., Pototzky, A. S., and Perry, B., III, "Computation of Maximized Gust Loads for Nonlinear Aircraft Using Matched-Filter-Based Schemes," *Journal of Aircraft*, Vol. 30, No. 5, 1993, pp. 763–768.

[3]Lee, Y. N., and Lan, C. E., "Analysis of Random Response with Nonlinear Unsteady Aerodynamics," *Journal of Aircraft*, Vol. 38, No. 8, 2000, pp. 1305–1312.

[4]Hoblit, F. M., *Gust Loads on Aircraft: Concepts and Application*, AIAA Education Series, AIAA, Washington, DC, 1988, pp. 29–46.

[5]Prewitt, N. C., Belk, D. M., and Maple, R. C., "Multiple Body Trajectory Calculations Using the Beggar Code," AIAA Paper 96-3384, July 1996.

[6]Hall, A., "Navier–Stokes/6-DOF Analysis of the JDAM Store Separation from the F/A-18C Aircraft," AIAA Paper 99-0121, Jan. 1999.

[7]Sickles, W. L., Denny, A. G., and Nichols, R. H., "Time-Accurate CFD Predictions for JDAM Separation from an F-18C Aircraft," AIAA Paper 2000-0796, Jan. 2000.

[8]Bagai, A., Leishman, J. G., and Park, J., "Aerodynamic Analysis of a Helicopter in Steady Maneuvering Flight Using a Free-Vortex Rotor Wake Model," *Journal of the American Helicopter Society*, Vol. 144, No. 2, 1999, pp. 109–120.

[9]Yang, G. W., Obayashi, S., and Nakamichi, J., "Aileron Buzz Simulation Using an Implicit Multiblock Aeroelastic Solver," *Journal of Aircraft*, Vol. 40, No. 3, 2003, pp. 580–589.

[10]Sakata, K., "Supersonic Experimental Airplane Program in NAL and its CFD-Design Research Demand," *Proceedings of the 2nd International CFD Workshop for Super-Sonic Transport Design*, Tokyo, Japan, July 2000.

[11]Thomas, P. D., and Lombard, C. K., "Geometric Conservation Law and Its Application to Flow Computations on Moving Grids," *AIAA Journal*, Vol. 17, No. 10, 1979, pp. 1030–1037.

[12]Baldwin, B. S., and Lomax, H., "Thin Layer Approximation and Algebraic Model for Separated Turbulent Flow," AIAA Paper 78-0257, Jan. 1978.

[13]Yoon, S., and Jameson, A., "Lower-Upper Symmetric Gauss–Seidel Method for the Euler and Navier–Stokes Equations," *AIAA Journal*, Vol. 26, No. 9, 1988, pp. 1025, 1026.

[14]Obayashi, S., and Guruswamy, G. P., "Convergence Acceleration of a Navier–Stokes Solver for Efficient Static Aeroelastic Computations," *AIAA Journal*, Vol. 33, No. 6, 1995, pp. 1134–1141.

[15]Yang, G. W., Kondo, M., and Obayashi, S., "Multiblock Navier–Stokes Solver for Wing/Fuselage Transport Aircraft," *JSME International Journal*, Series B, Vol. 45, No. 1, 2002, pp. 85–90.

[16]Bisplinghoff, R. L., Ashley, H., and Halfman, R. L., *Aeroelasticity*, Addison Wesley Longman, Reading, MA, 1955, Chap. 3, pp. 151–162.

[17]Yang, G. W., and Obayashi, S., "Transonic Aeroelastic Calculation with Full Implicit Subiteration and Deforming Grid Approach," *Proceedings of the Aeronautical Numerical Simulation Technology Symposium 2001*, Tokyo, Japan, May 2001.